

Supporting Information for
Permeation Pathways through Lateral Domains
in Model Membranes of Skin Lipids

Annalaura Del Regno* and Rebecca Notman*

Department of Chemistry, The University of Warwick, Coventry, United Kingdom

E-mail: annalaura.del-regno@stfc.ac.uk; r.notman@warwick.ac.uk

Bilayer Set-up

The composition of the systems studied is shown in Table S1. The molecular dynamics (MD) protocol used to prepare our model bilayers is reported in Table S2.

Table S1: Composition of the four lipid bilayer systems simulated in this work.

CER[NS]24:CHOL:FFA24 (molar ratio)	$n_{\text{CER[NS]24}}$	n_{CHOL}	n_{FFA}
1:1:1*	60	60	60
1:1:1†	120	120	120
2:2:1*	72	72	36
2:2:1†	144	144	72

*Fully hydrated model (FH), lipid:H₂O ratio of 1:30 (~ 5428 H₂O)

†Low hydration model (LH), lipid:H₂O ratio of 1:2 (~ 720 H₂O).

Table S2: MD simulation protocol.

Anhydrous lipid bilayer				
Stage	Ensemble	Temperature /K	Restrains*	Duration /ns
1	NPT , 1 bar _{x,y} - 0 bar _{z}	305	z direction	2
2	NVT	600	z direction	40
3	NVT	305	z direction	5
Hydrated lipid bilayer				
Stage	Ensemble	Temperature /K	Restrains*	Duration /ns
4a†	NVT	305	z direction	2
4b	NPT , 1 bar _{x,y} - 2 bar _{z}	305	—	0.1
5	NPT 1 bar _{x,y} - 1 bar _{z}	305	—	47

*A harmonic restraint of 1000 kJ mol⁻¹ was applied to lipid atoms only.

†This step was performed for the low hydration systems only.

Structural Properties of the Bilayers

Structural properties are summarized in Table S3.

Table S3: Area per lipid, tilt angle and bilayer thickness for FH and LH models, collected over the last 25 ns of Stage 5 (Table S2) and averaged over three independent simulations. The vectors used to calculate the tilt angles are shown in Figure S2.

Fully hydrated lipid bilayer			
Property		Composition (CER[NS]24:CHOL:FFA24)	
		1:1:1	2:2:1
Area per lipid /Å ²	CER[NS]24	32.43(44)	35.01(32)
	CHOL	31.19(39)	34.40(34)
	FFA24	27.47(42)	28.88(54)
	Average	30.37(2)	33.54(3)
Tilt angle /°	CER	12.37(86)	14.28(88)
	CHOL	7.46(71)	8.30(52)
	FFA24	11.60(79)	13.25(1.13)
	CER[NS]24 headgroup	94.90(3.60)	93.82(3.10)
Bilayer thickness /nm		4.76(3)	4.55(2)

Low hydration lipid bilayer			
Property		Composition (CER[NS]24:CHOL:FFA24)	
		1:1:1	2:2:1
Area per lipid /Å ²	CER[NS]24	33.24(25)	34.60(16)
	CHOL	32.12(27)	34.18(18)
	FFA24	28.18(30)	29.01(30)
	Average	31.18(3)	33.31(3)
Tilt angle /°	CER[NS]24	13.84(1.01)	14.59(95)
	CHOL	8.82(61)	8.42(53)
	FFA24	13.01(89)	13.50(1.19)
	CER[NS]24 headgroup	96.47(3.54)	94.75(3.28)
Bilayer thickness /nm		4.65(2)	4.57(2)

For all the analyses reported below, configurations of the system were collected every 5 ps and averaged over the final 25 ns of the simulation and over three independent simulations of each bilayer system. The area per lipid (APL), bilayer thicknesses and lipid tilt angles were calculated using the MEMBPLUGIN¹ developed for VMD.²

Area per lipid

The APL was calculated by selecting a representative headgroup atom for each lipid and then projecting the xy coordinates of each selected atom onto the xy plane of the simulation box. The projection was then used to construct a Voronoi diagram and the area of each polygon calculated. Each polygon was attributed to one of the three lipid species and used to compute an average area per lipid species. In this work we selected the headgroup nitrogen atom for the ceramide 2 molecules (CER[NS]24), the hydroxyl oxygen for the CHOL and the carboxylic oxygen for the C24 fatty acid (FFA24).

The average APL for the systems and the components are reported in Table S3. The evolution of the average APL of our bilayers and the APL of each membrane component over the last 25 ns of the simulation are shown in Figure S1. All the APLs converge over the simulated time, as shown in Figure S1. In general the APL increases in the order FFA24 < CHOL < CER[NS]24. This result was expected, as FFA24 is composed of only one alkyl chain and thus has a smaller projection onto the xy plane compared to the CER[NS]24 and the bulkier CHOL. Simulations of mixed free fatty acid and CHOL bilayers have shown, in fact, an even smaller average APL than those observed in this work (mixtures of 50% in weight of stearic and palmitic acid with CHOL show an average APL of $\sim 22 \text{ \AA}^2$).³ Our results therefore suggest that CER[NS]24 has an influence on the way CHOL and free fatty acids pack together in a bilayer.

CHOL shows an average APL remarkably close to the CER[NS]24 in every system (Table S3). This is consistent with the observation of Plesnar et al.⁴ who report a value of 38 \AA^2 for the APL of CHOL in a pure CHOL bilayer simulated at 300 K, comparable with the APL of a pure CER[NS]24 bilayer (38.9 \AA^2) simulated at the same conditions.⁵ In general the average APLs of the mixed systems are lower than those observed for the pure CER[NS]24 systems (Notman et al.⁶ reported values of APL equal to 36.6 ± 0.1 at 283 K, 37.4 ± 0.2 at 323 K and $38.8 \pm 0.5 \text{ \AA}^2$ at 363 K while Das et al.⁵ reported an APL value for pure CER[NS]24 of $\sim 38.9 \text{ \AA}^2$ at 300 K). In pure CER[NS]24 bilayers, the lipids pack in a hexagonal arrange-

ment, where a strong network of hydrogen bonds (H-bonds) is created between adjacent lipid headgroups and with water molecules.⁶ In the case of mixed bilayers, no significant long-range hexagonal arrangement is observed, consistent with the experimental observation of Bouwstra et al.;⁷ furthermore, both CHOL and FFA24 have a smaller number of H-bond donor/acceptor groups than CER[NS]24, leading to a slightly more flexible system.

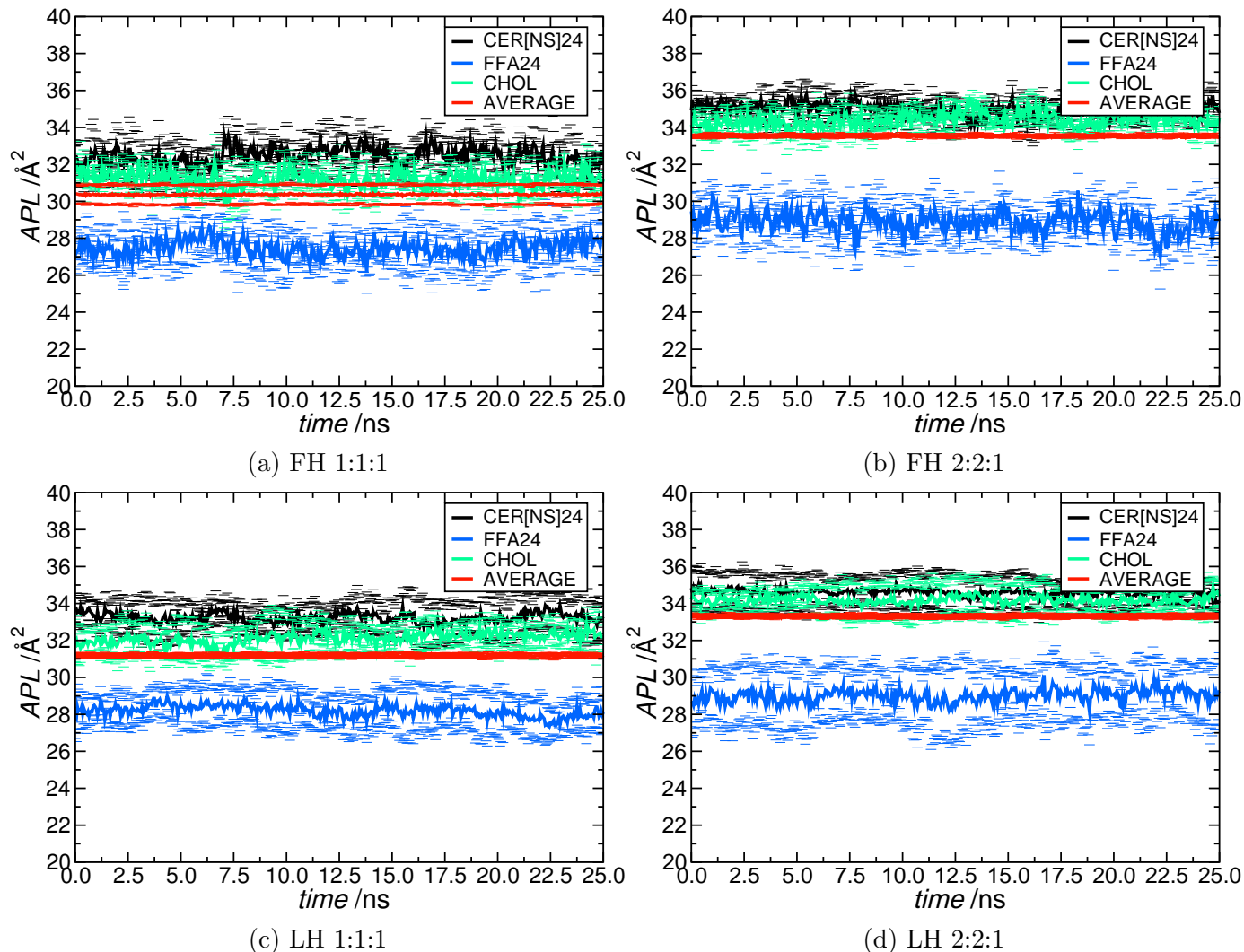


Figure S1: APL for the FH 1:1:1, FH 2:2:1, LH 1:1:1 and LH 2:2:1 bilayers. The average APL is shown in red, CER[NS]24 in black, CHOL in green and FFA24 in blue. Error bars are shown as standard deviation from the average value.

Bilayer thickness

The thickness computation for each frame of the trajectory was based on the mass distributions for selected atoms. The projections of the masses onto the z -axis gave two peaks and the distance between the peaks was taken as the thickness of the bilayer. In this work the headgroup nitrogen atom of the CER[NS]24 was used as the reference atom. Average thicknesses for the systems are reported in Table S3. In general, the thicknesses of the mixed bilayers are smaller than those estimated for the pure CER[NS]24 (~ 49 Å).⁶ When the lipid ratio changes from 1:1:1 to 2:2:1, the thickness decreases; the opposite trend is observed for the APL. A small variation in both thickness and APL is observed when the water concentration is changed, particularly in the case of the 1:1:1 LH bilayer; in this situation the thickness decreases while the APL slightly increases; no relevant differences are observed between FH and LH in the 2:2:1 system. This is the result of the different tilt angles observed for each of the system studied (see below and Table S3).

Tilt angles

The lipid tilt angles are defined as the angle between the vectors defined in Figure S2 and the normal to the bilayer. Average tilt angles for the different lipid species in each system are reported in Table S3. It is evident that in the LH 1:1:1 bilayer the lipids are more tilted relative to the bilayer normal, than in the FH bilayer. We suggest that this is due to the formation of water pools, which can cause a local distortion of the bilayer. In the case of the 2:2:1 bilayers, no relevant differences in tilt angles are observed by changing hydration level, and consequently we found no appreciable variations in the thickness.

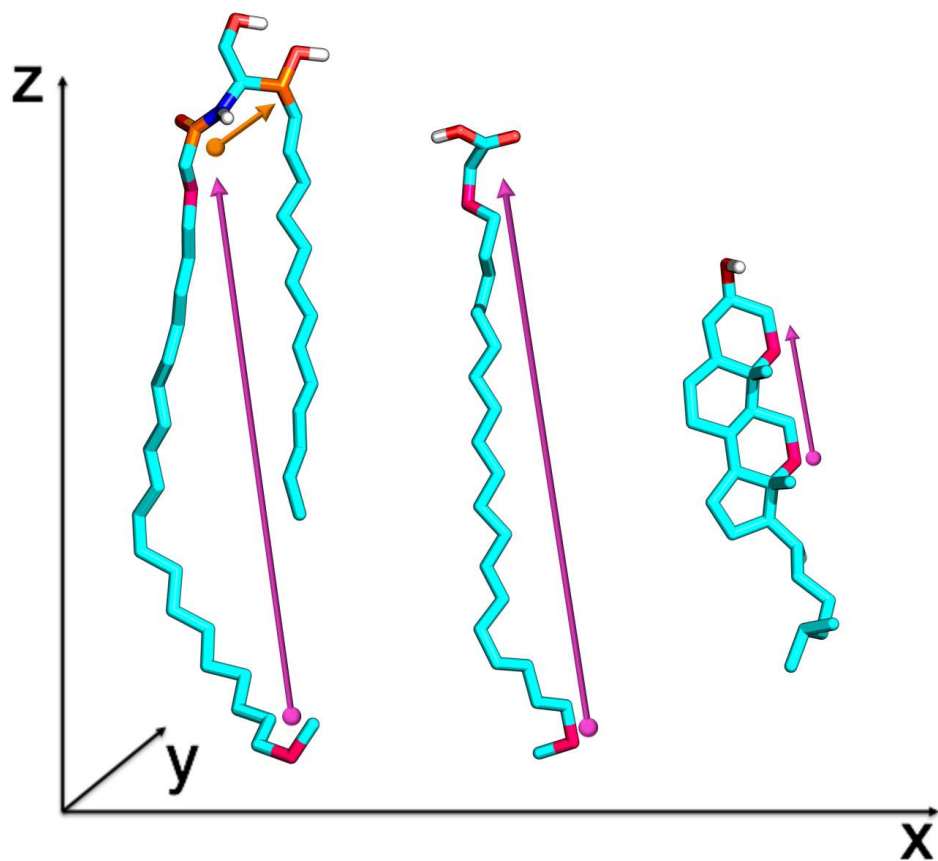


Figure S2: From the left, CER[NS]24, FFA24 and CHOL molecules are shown. Carbon atoms are coloured in cyan, oxygen in red, hydrogen in white and nitrogen in blue. The atoms used to define the tilt vectors are coloured in pink; the vector for the CER[NS]24 head tilt angle is defined by the atoms coloured in orange.

Lipid conformation

The different conformations assumed by the lipids in the mixed systems are shown in Figures S3-S5. The CER[NS]24 molecules can assume a series of different conformations (Figure S3) where the C24 chain is either bent (Figure S3 a and b) or retracted at the water interface (Figure S3c and d). Such behaviour, previously reported for pure CER[NS]24 bilayers,^{5,6} is a mechanism used by the ceramides to pack uneven alkyl chains, instead of interdigitating. Given the behaviour of the CER[NS]24 lipids, FFA24 molecules have to pack a relatively long chain (C24) in a less favourable environment; in this situation, FFA24 assumes bent conformations (Figure S4a-b), similar to those observed for the CER[NS]24. In some cases we also observed the bending of the fatty acid at the interface (Figure S4c and e) with an associated formation of H-bonds with either CER[NS]24 or CHOL lipids situated below the interface. In the FH 1:1:1 system, CHOL molecules are found slightly below the interface, and sometimes they diffuse to the centre of the bilayer and lie perpendicular to the normal of the bilayer (Figure S5); similar behaviour has been recently reported by Das et al.⁸ over a 1 μ s molecular dynamics simulation of a stacked bilayer at 340 K. This behaviour is not observed in the FH 2:2:1 bilayer, nor in the LH systems in our simulation time.

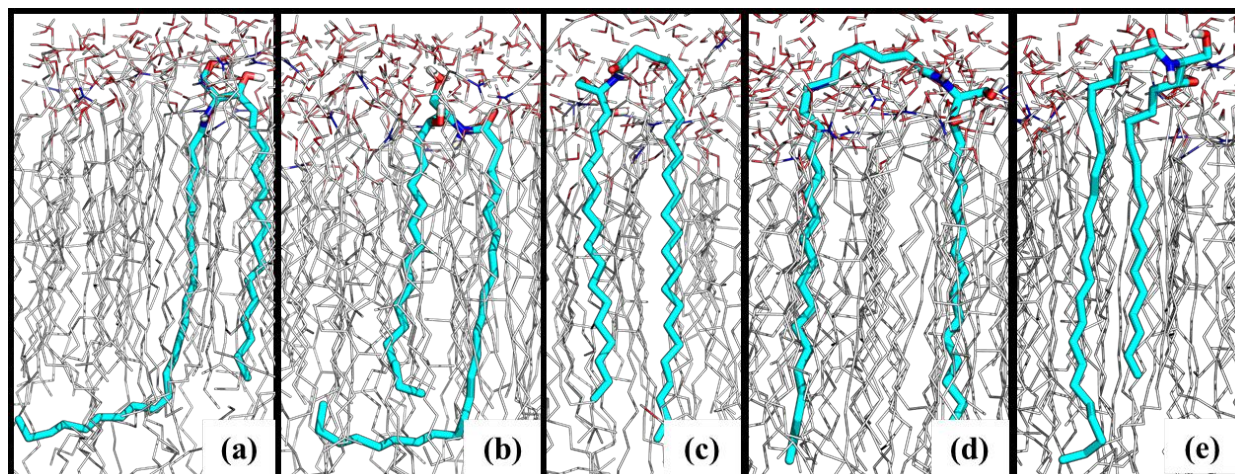


Figure S3: Snapshots from the simulation of the FH 1:1:1 bilayer at 305 K showing examples of the different CER[NS]24 conformations. The molecules of interest are shown as sticks; carbon atoms are cyan, oxygen red, nitrogen blue and hydrogen white.

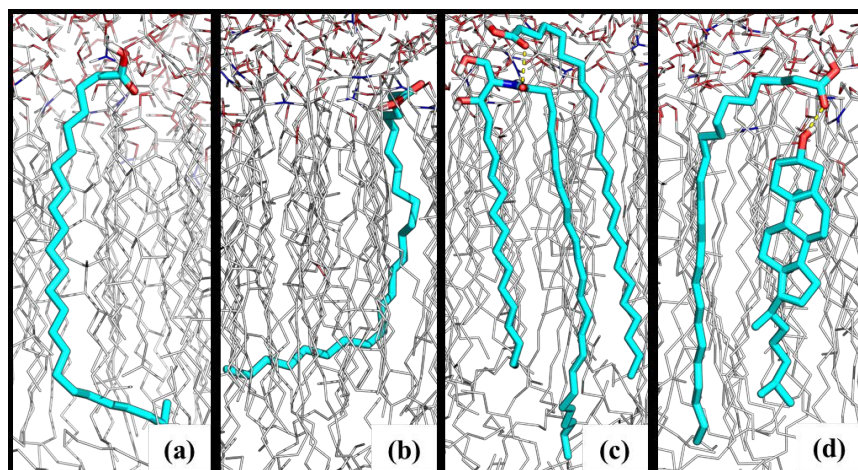


Figure S4: Snapshots from the simulation of the FH 1:1:1 bilayer at 305 K showing examples of the different FFA24 conformations. The molecules of interest are shown as sticks; carbon atoms are cyan, oxygen red, nitrogen blue and hydrogen white.

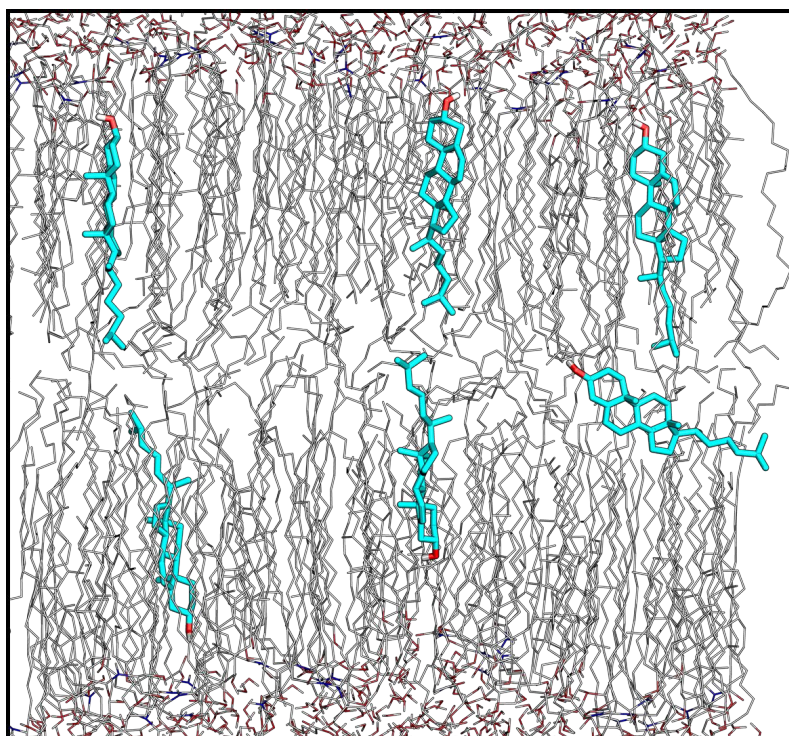


Figure S5: Snapshot from the simulation of the FH 1:1:1 bilayer at 305 K showing examples of CHOL behavior in the bilayer. The molecules of interest are shown as sticks; carbon atoms are cyan, oxygen red and hydrogen white.

Density profiles

The density profiles for the FH and the LH lipid bilayers are shown in Figure S6. The density of each bilayer component was calculated using the *g_density* tool in Gromacs.⁹ In general the profiles are fairly similar between systems with the same level of hydration. In the FH systems, moving from the bulk water to the centre of the bilayer we observe, at first, a flat line corresponding to the water density; as we approach the bilayer, the water density decreases while the densities of CER[NS]24 and FFA24 start to increase. The region where the water and the lipids overlap corresponds to the headgroup region of the bilayer where the density profile of the nitrogen atom of the CER[NS]24 is at its maximum. The CHOL density starts increasing significantly when we reach the tail-group region, and diminishes around the centre of mass of the bilayer. In this area we observed a shoulder in the density profile of both CER[NS]24 and FFA24; this shoulder corresponds to the density of bent alkyl chains discussed earlier.

The density profiles of LH systems are fairly similar to the FH density profiles for the main body of each bilayer, but present small differences from the FH at the interfaces. First, the overlap region between the water and the lipids is broader than in the case of FH, especially for the LH 1:1:1 system. This is an artefact due to the formation of small water pools. In areas where water is absent, the lipids of adjacent bilayers can interact and create a network of H-bonds. In particular, the FFA24 tends orient at the interface of the pool surrounding the hydrophilic area, resulting in an overlap of the FFA24 and water densities. It is worth emphasising that in the case of the LH 1:1:1 bilayer, only one peak corresponding to the density of FFA24 is found at the interface; whereas two shoulders are observed in the case of the LH 2:2:1 bilayer, corresponding to the heads of the lipids belonging to different bilayers. These two shoulders are seen in every system for the CER[NS]24 suggesting that CER[NS]24 tends to remain in the bilayer it began the simulation in, rather than the more flexible FFA24 which can protrude into the adjacent bilayer.

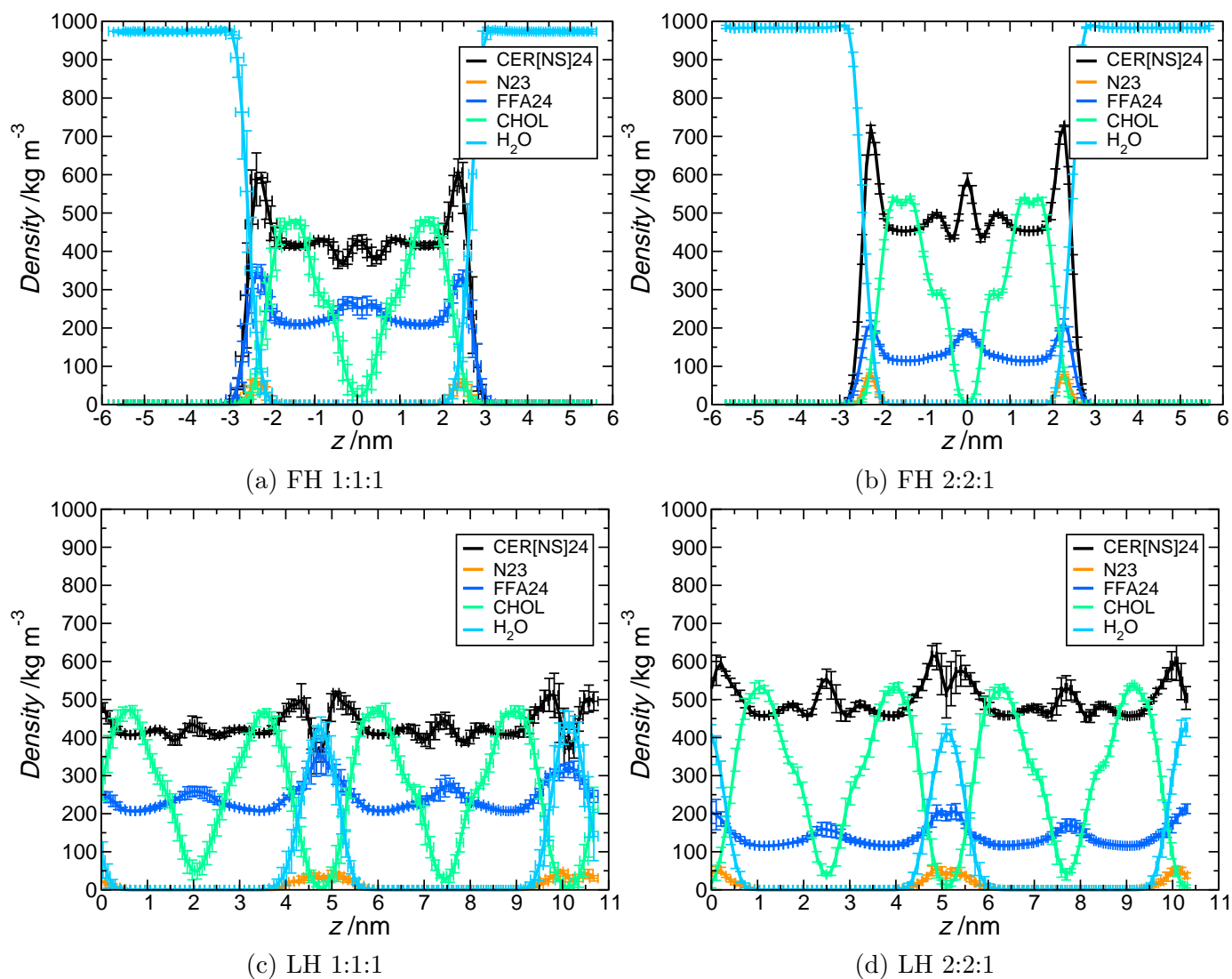


Figure S6: Density profiles for CER[NS]24, FFA24, CHOL and water. CER[NS]24 is coloured in black, the ceramide N atom in orange, CHOL in green, FFA24 in blue and water in cyan.

Order parameters

The lipid-tail-order parameter S_Z for hydrocarbon tail atom C_n was calculated using the built in *g_order* tool in Gromacs.⁹ S_Z is defined as

$$S_z = \frac{3}{2}\cos^2(\theta_Z) - \frac{1}{2} \quad (1)$$

where θ_Z is the angle between the z axis of the simulation cell and the vector C_{n-1} to C_{n+1} . The order parameters for the FH and LH systems are shown in Figure S7. The order parameter profiles for all the bilayers are almost identical, with the exception of the FH 1:1:1 system, which appears to be more ordered than the others. This may be an artefact due to the different tilting of the lipids in this bilayer. In general, the CER[NS]24 C16 tail is more ordered in its central region, whereas a slightly higher disorder is found at the beginning and at the end of the alkyl chains, close to the centre of the bilayer. Overall the C24 tails are more disordered than the C16 tails, and they follow the same shape as the FFA24 chains, suggesting that the latter assumes a similar conformation to the CER[NS]24 C24 tails. A high degree of disorder is found at the core region of the bilayer and at the interface with water, where the chains are almost parallel to the normal.

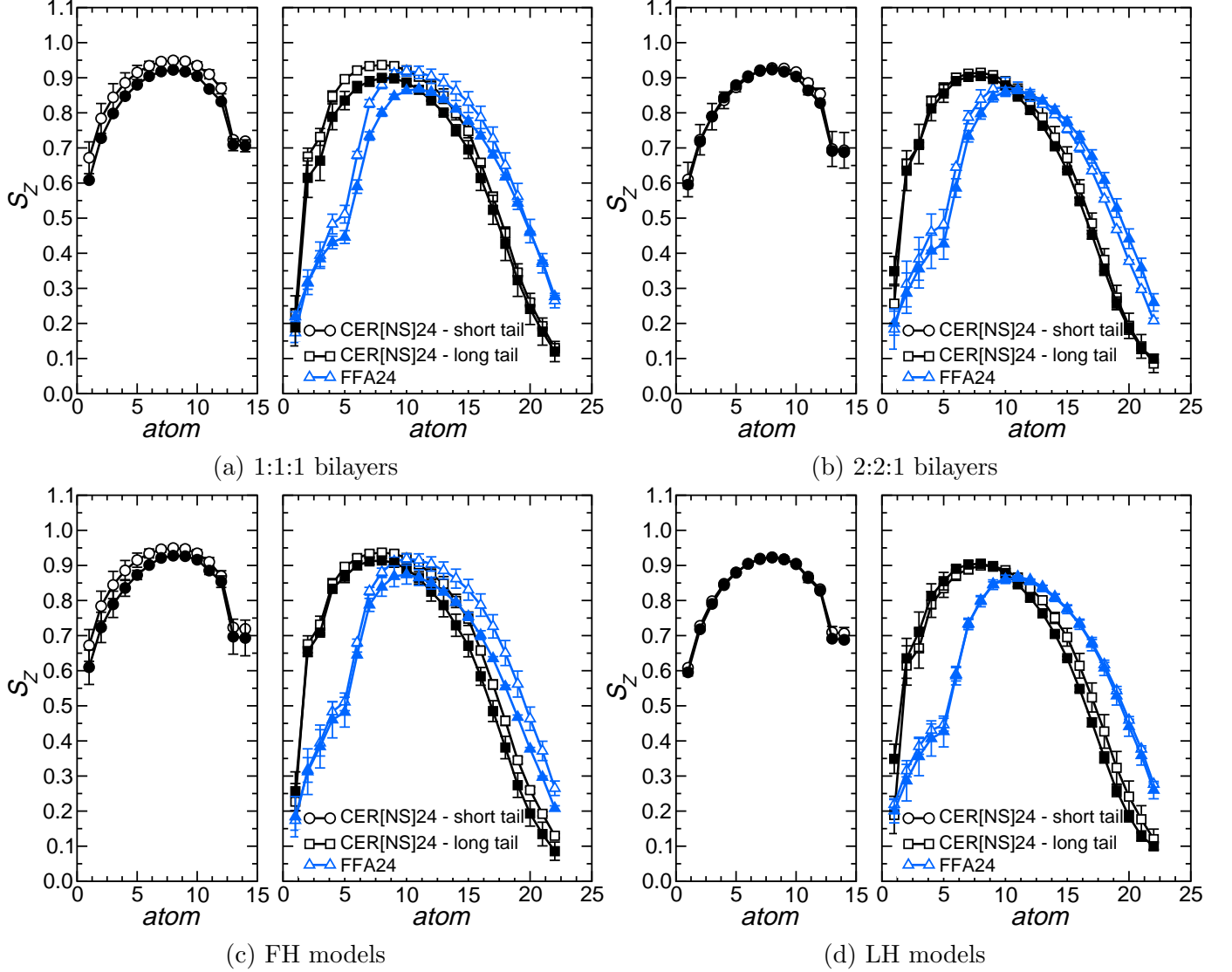
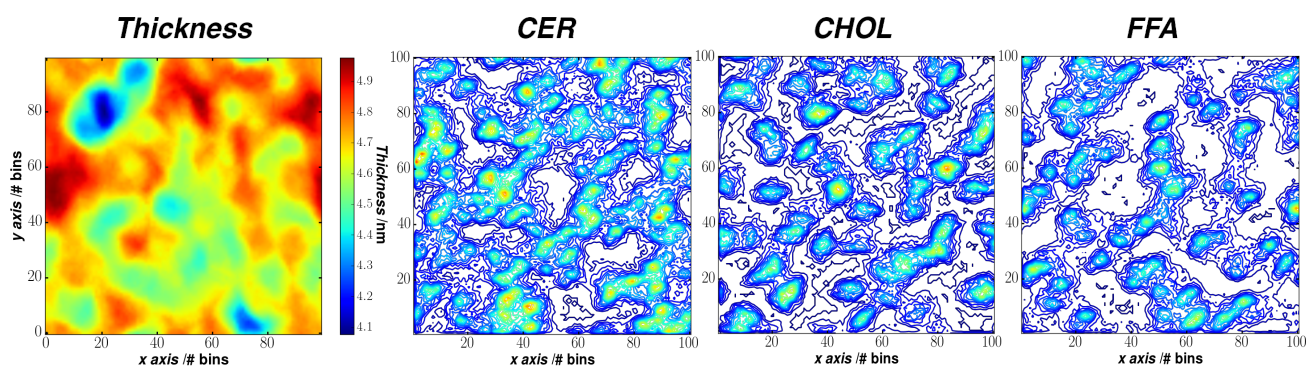


Figure S7: Order parameters for the different bilayer models. Figure (a): order parameters for the FH (empty symbols) and LH (fully symbols) 1:1:1 models. Figure (b): order parameters for the FH (empty symbols) and LH (fully symbols) 2:2:1 models. Figure (c): order parameters for the FH 1:1:1 (empty symbols) and 2:2:1 (fully symbols) models. Figure (d): order parameters for the LH 1:1:1 (empty symbols) and 2:2:1 (fully symbols) models.

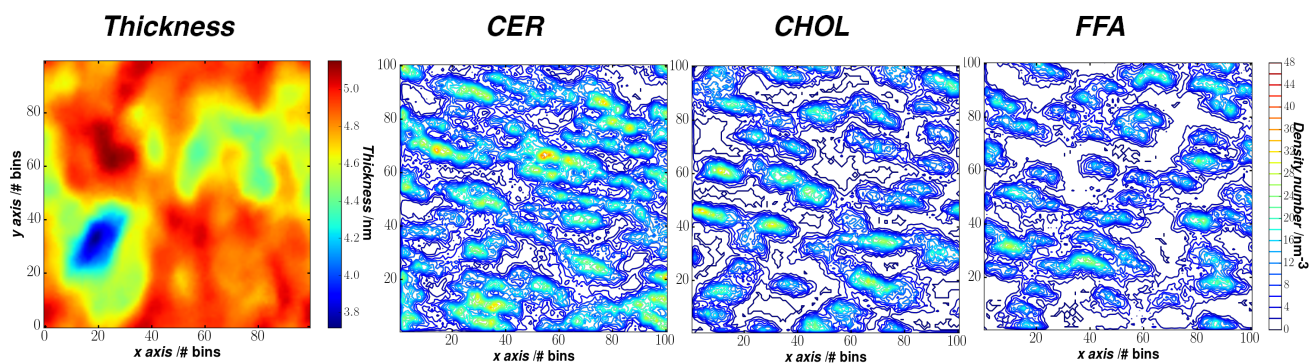
2D thickness and number density maps for the FH models

2D thickness and number density maps (CER[NS]24, CHOL and FFA24) for the FH 1:1:1 and FH 2:2:1 bilayers are shown in Figures S8 and S9.

The thickness was calculated using the the *g_lomepro* package¹⁰ developed for Gromacs.⁹ 2D number density maps were calculated in the *xy* plane using the *g_densmap* tool in Gromacs.⁹

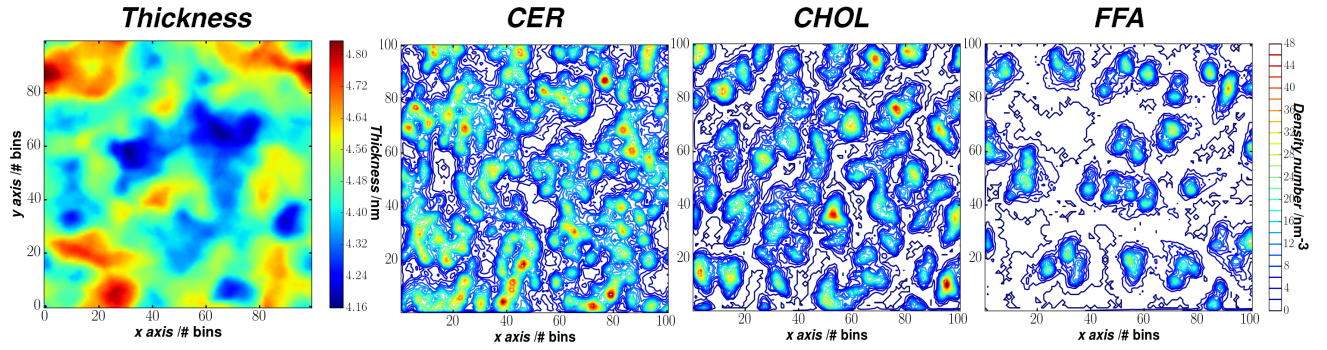


(a) 1:1:1 FH bilayer - sample 2

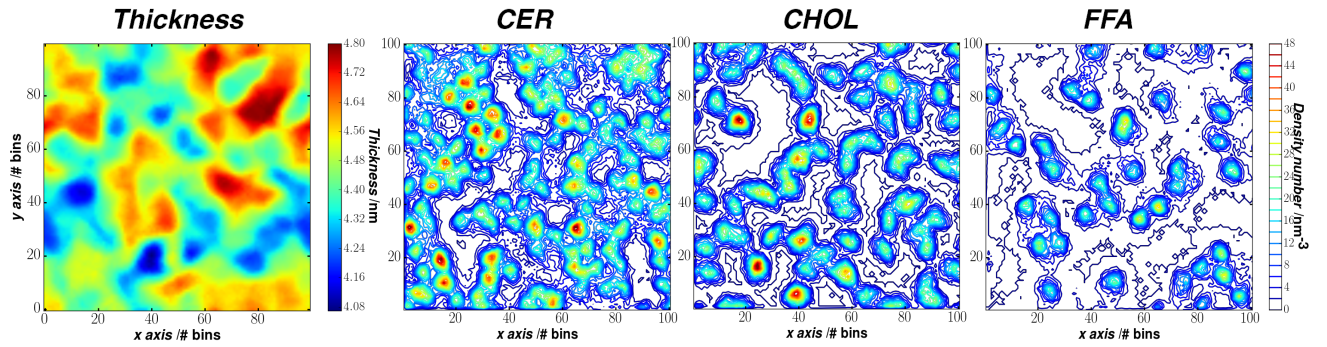


(b) 1:1:1 FH bilayer - sample 3

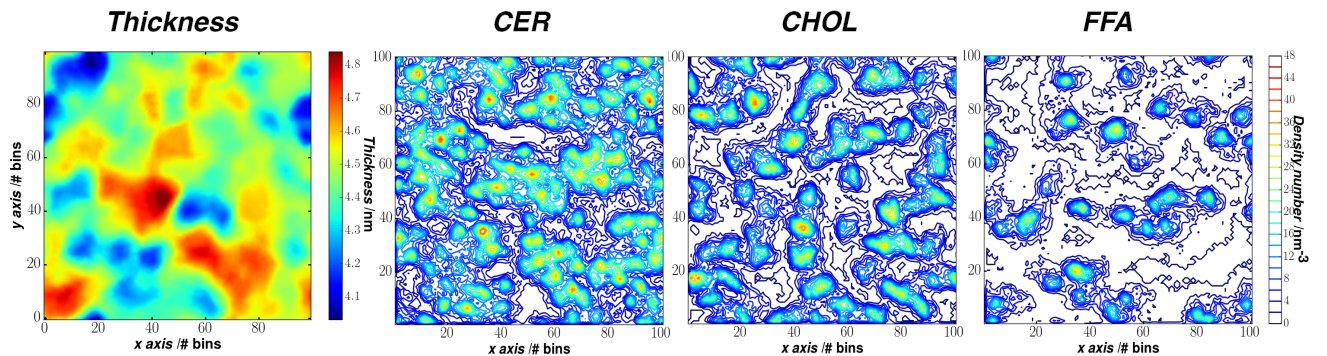
Figure S8: 2D thickness map and 2D CER[NS]24, CHOL and FFA24 number density maps are shown for the FH 1:1:1 bilayers, samples 2-3.



(a) 2:2:1 FH bilayer - sample 1



(b) 2:2:1 FH bilayer - sample 2



(c) 2:2:1 FH bilayer - sample 3

Figure S9: 2D thickness map and 2D CER[NS]24, CHOL and FFA24 number density maps are shown for the FH 2:2:1 bilayers, samples 1-3.

Cluster analysis

In this work, molecules are considered to belong to the same cluster when a partial overlap of the Van der Waals radii of their particles occurs. An in-house code was prepared to analyse the lateral phase behaviour of the lipids in each leaflet. The code was written in the Python language and uses the MDanalysis, NetworkX and Matplotlib packages.¹¹⁻¹³ At every nanosecond of the trajectory, the nearest neighbours are found by calculating the distances D_{ij} between all pairs of particles i and j . Intervals of 1 ns were chosen to reduce the effect of small fluctuations in the distances between molecules on short timescales.

If

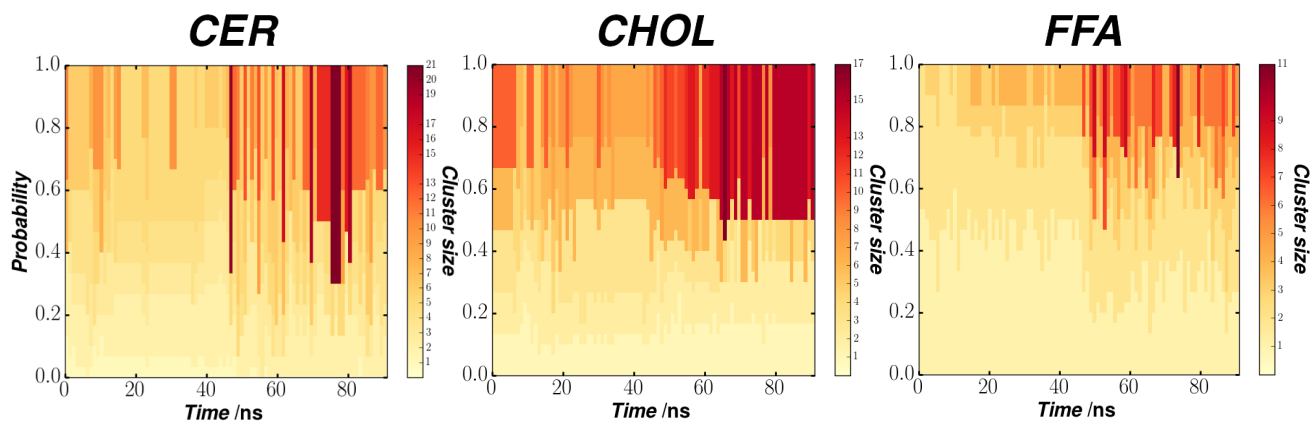
$$D_{ij} < 0.72(R_i + R_j) \tag{2}$$

where R_i and R_j are the Van der Waals radii of the particles, the atoms are considered connected. At this point if connected atoms belong to two different molecules, then the molecules are considered to be touching. To monitor the evolution of clusters through the simulations, the connections between residues are used as edges in a graph, with the resulting unconnected subgraphs forming the clusters. The cluster size is then simply the number of nodes (molecules) in each graph.

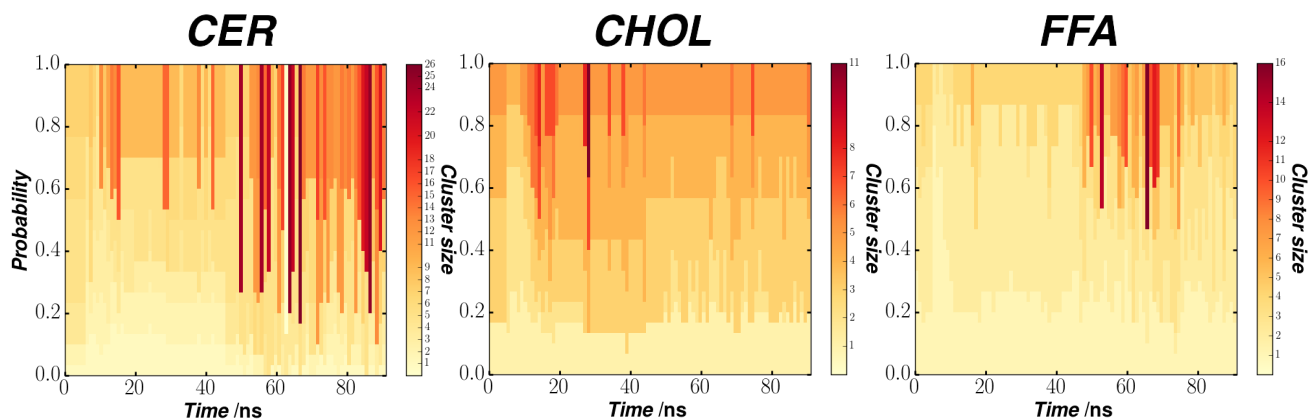
The evolution of the cluster sizes over time is shown in Figures S10-S12. The results were normalised by the number of each type of lipid in that leaflet, to give a probability between 0 and 1 of finding a cluster of a particular size. When looking at Figures S10-S12, it is evident that the CHOL molecules tend to form more stable agglomerates, which consistently grow through the simulation time. This behaviour is observed for at least one leaflet in all the samples analysed. FFA24 shows higher variability, where larger clusters are continuously formed and broken. CER[NS]24 instead, tends to form very long network across the entire membrane. These results are also confirmed by visual inspection of the trajectory (Figure S13).

At the end of the simulation of sample 1, we observed that the CHOL has a high probability

of having clusters composed of 7 and 15 in leaflet 1 (Figure S10a) while FFA24 has the highest probability of having clusters of 2 and 4. CER[NS]24, which is fairly spread through the system, also fluctuates between clusters of 7 and 15 molecules. The behaviour of the lipids is similar for leaflet 2 (Figure S10(b)), although smaller clusters are formed for CHOL and FFA24. A similar behaviour is observed for all our samples (Figure S11 and S12).

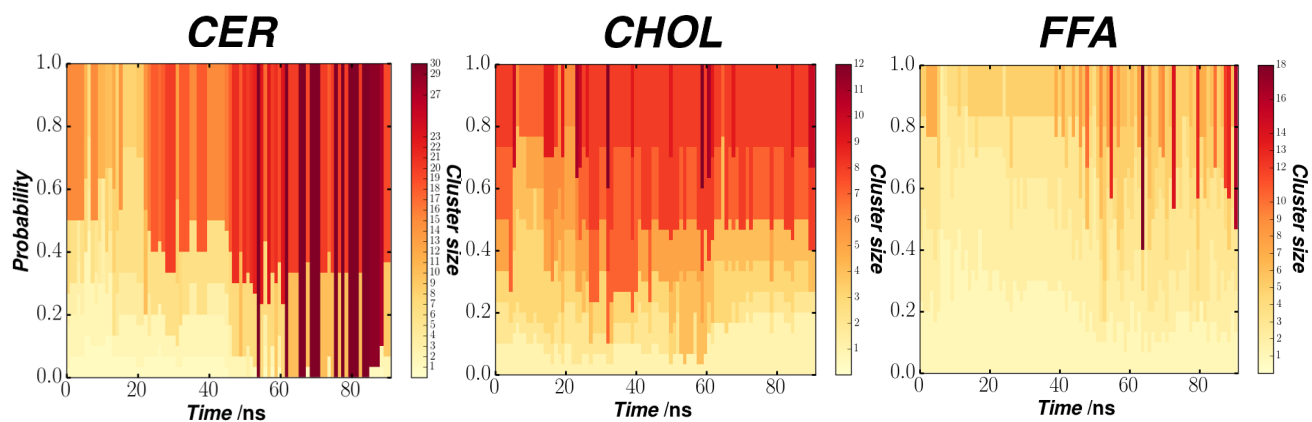


(a) 1:1:1 FH bilayer 1 - Leaflet 1

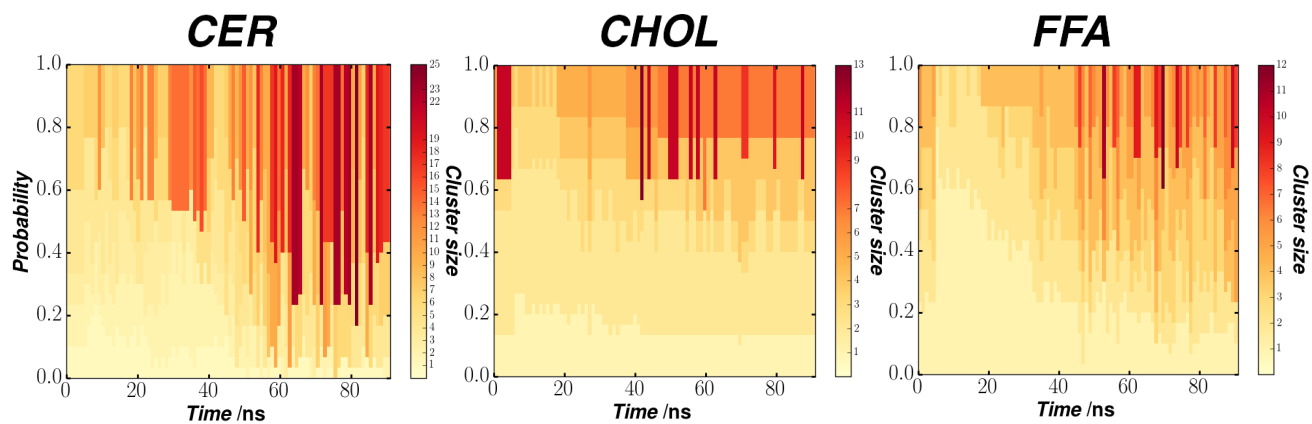


(b) 1:1:1 FH bilayer 1 - Leaflet 2

Figure S10: Cluster analysis of CER[NS]24, CHOL and FFA24, carried out for each leaflet of the FH 1:1:1 bilayer - sample 1.

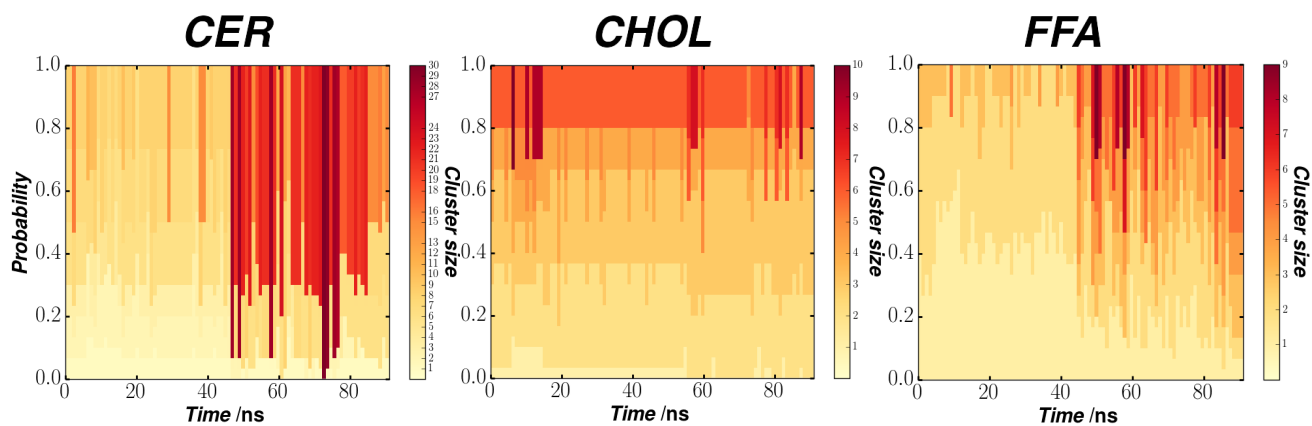


(a) 1:1:1 FH bilayer 2 - Leaflet 1

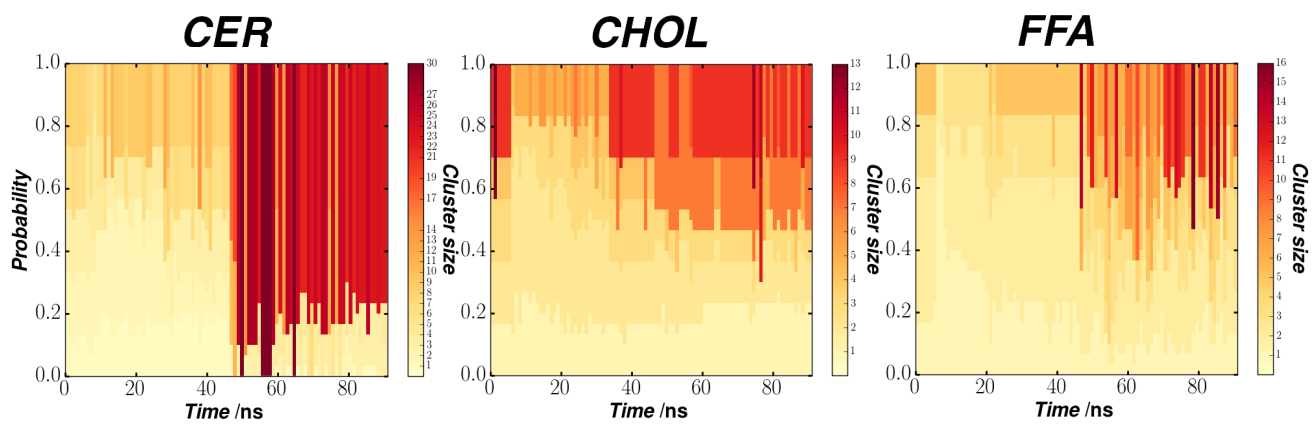


(b) 1:1:1 FH bilayer 2 - Leaflet 2

Figure S11: Cluster analysis of CER[NS]24, CHOL and FFA24, carried out for each leaflet of the FH 1:1:1 bilayer - sample 2.



(a) 1:1:1 FH bilayer 3 - Leaflet 1



(b) 1:1:1 FH bilayer 3 - Leaflet 2

Figure S12: Cluster analysis of CER[NS]24, CHOL and FFA24, carried out for each leaflet of the FH 1:1:1 bilayer - sample 3.

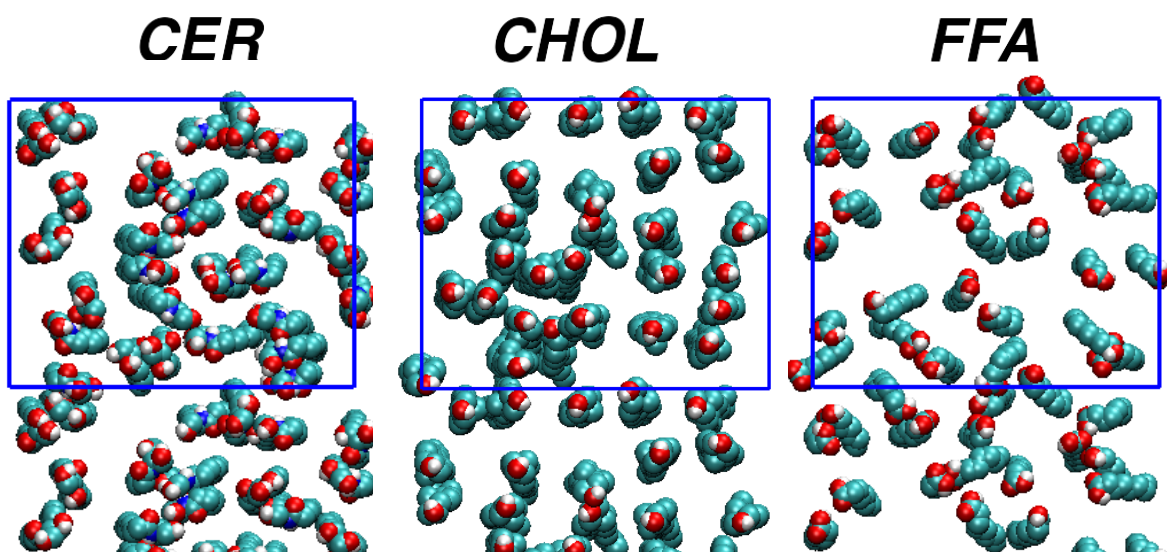


Figure S13: Final Snapshot for CER[NS]24, CHOL and FFA24 in leaflet 1 of FH 1:1:1 bilayer 1.

2D thickness and number density maps for the LH models

2D thickness and number density maps (CER[NS]24, CHOL and FFA24) for the LH 1:1:1 and LH 2:2:1 bilayers are shown in Figures S15-S19. 2D thickness maps of the LH bilayers versus the 2D number density maps of water are reported in Figures S20-S24.

The thickness was calculated using the the *g_lomepro* package¹⁰ developed for Gromacs.⁹ 2D number density maps were calculated in the *xy* plane using the *g_densmap* tool in Gromacs.⁹

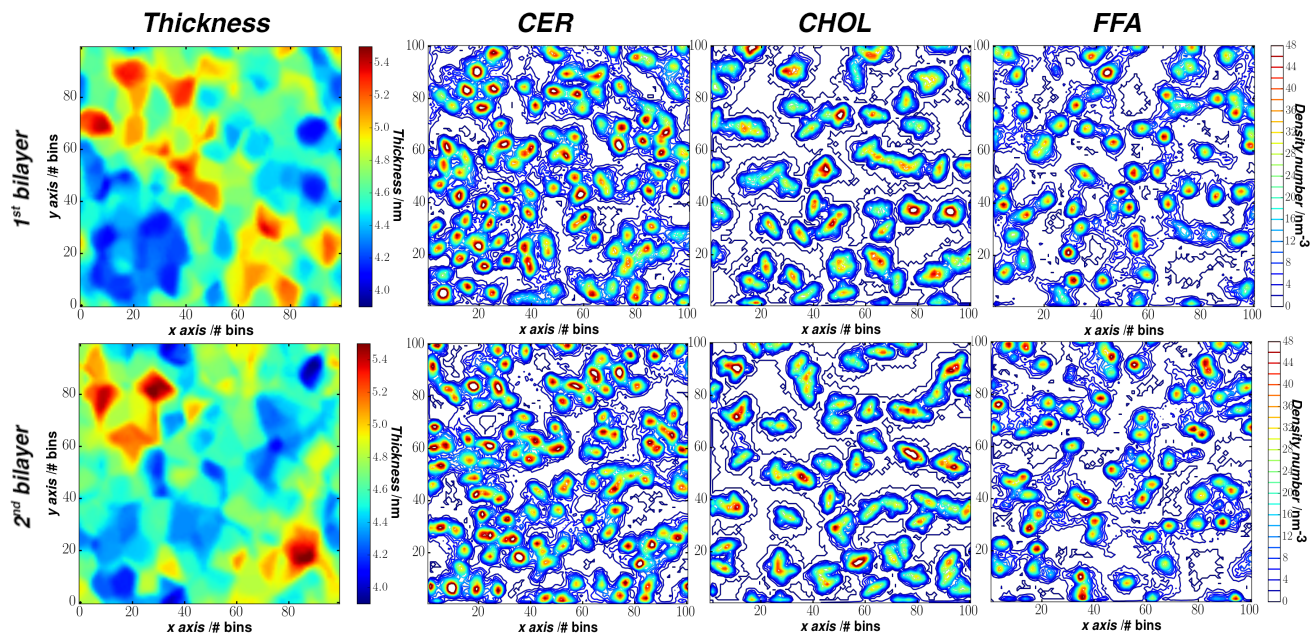


Figure S14: 2D thickness map and 2D CER[NS]24, CHOL and FFA24 number density maps are shown for sample 1, 1:1:1 LH bilayer; On the left the 2D thickness maps are shown for the bilayers composing the systems while 2D number density maps for each components are shown on the right.

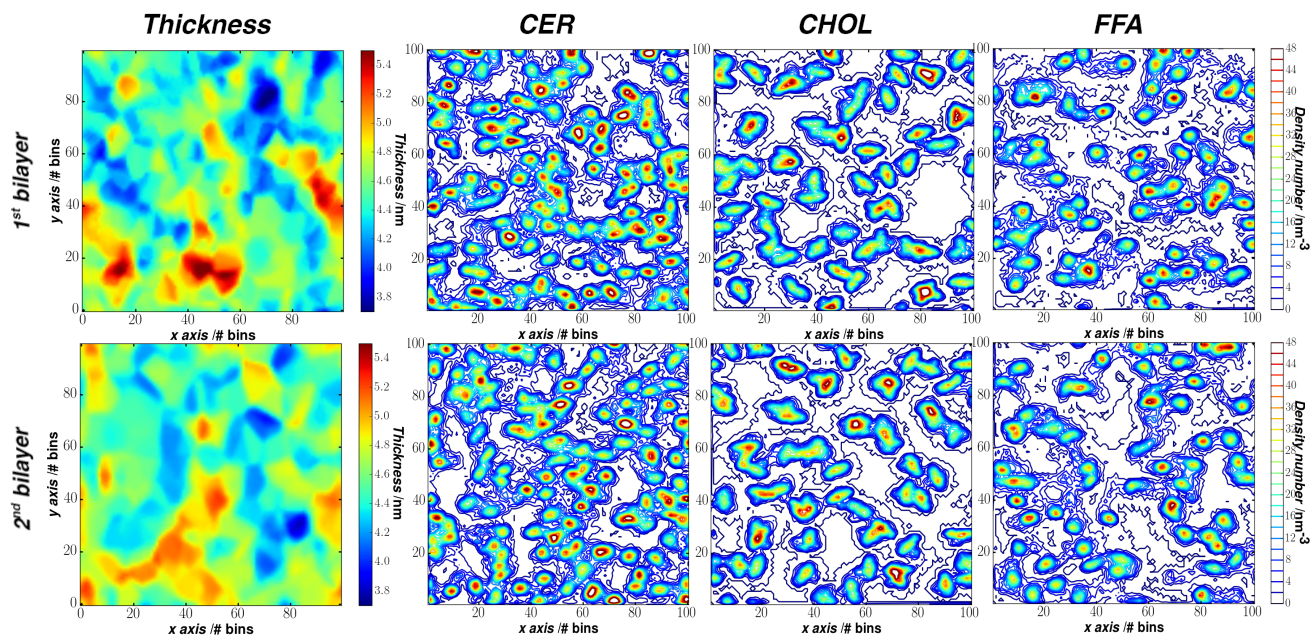


Figure S15: 2D thickness map and 2D CER[NS]24, CHOL and FFA24 number density maps are shown for sample 2, 1:1:1 LH bilayer; On the left the 2D thickness maps are shown for the bilayers composing the systems while 2D number density maps for each components are shown on the right.

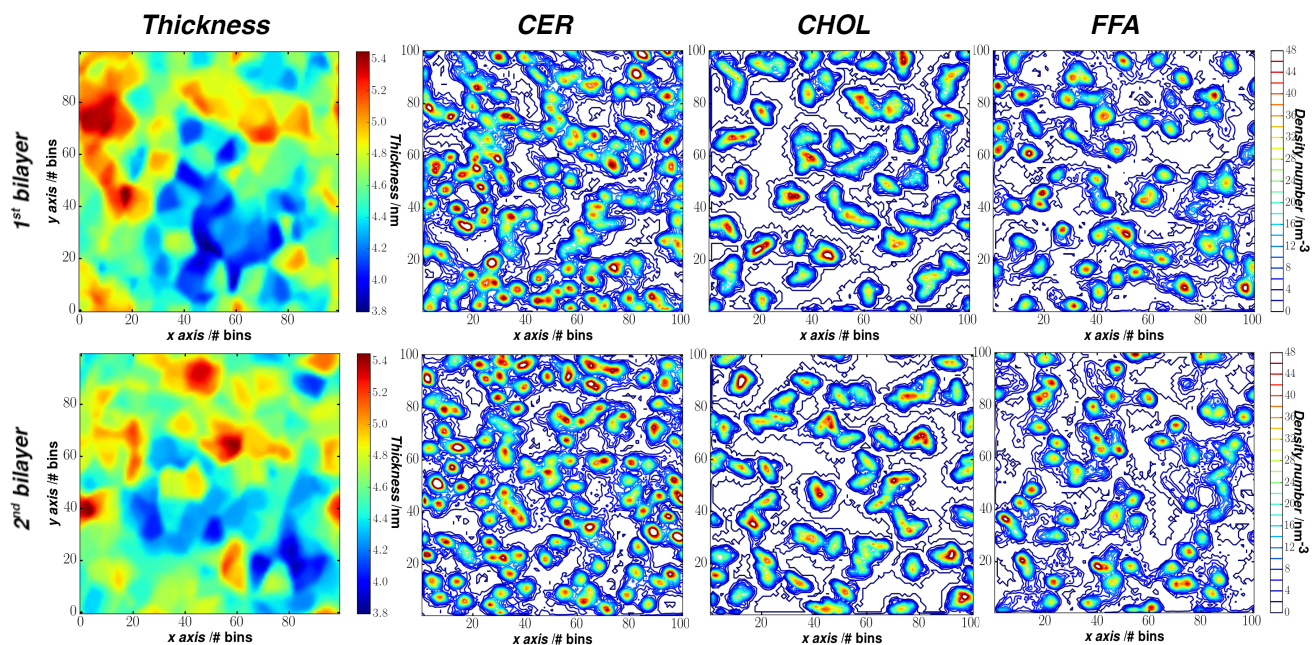


Figure S16: 2D thickness map and 2D CER[NS]24, CHOL and FFA24 number density maps are shown for sample 3, 1:1:1 LH bilayer; On the left the 2D thickness maps are shown for the bilayers composing the systems while 2D number density maps for each components are shown on the right.

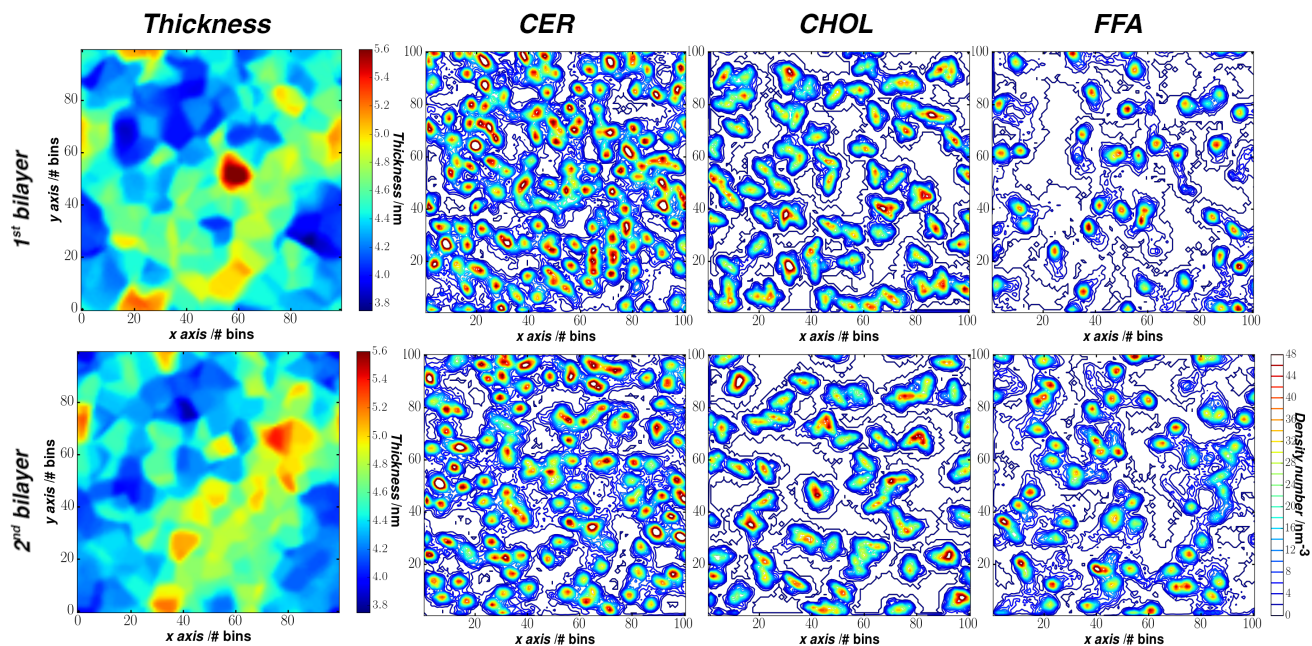


Figure S17: 2D thickness map and 2D CER[NS]24, CHOL and FFA24 number density maps are shown for sample 1, 2:2:1 LH bilayer; On the left the 2D thickness maps are shown for the bilayers composing the systems while 2D number density maps for each components are shown on the right.

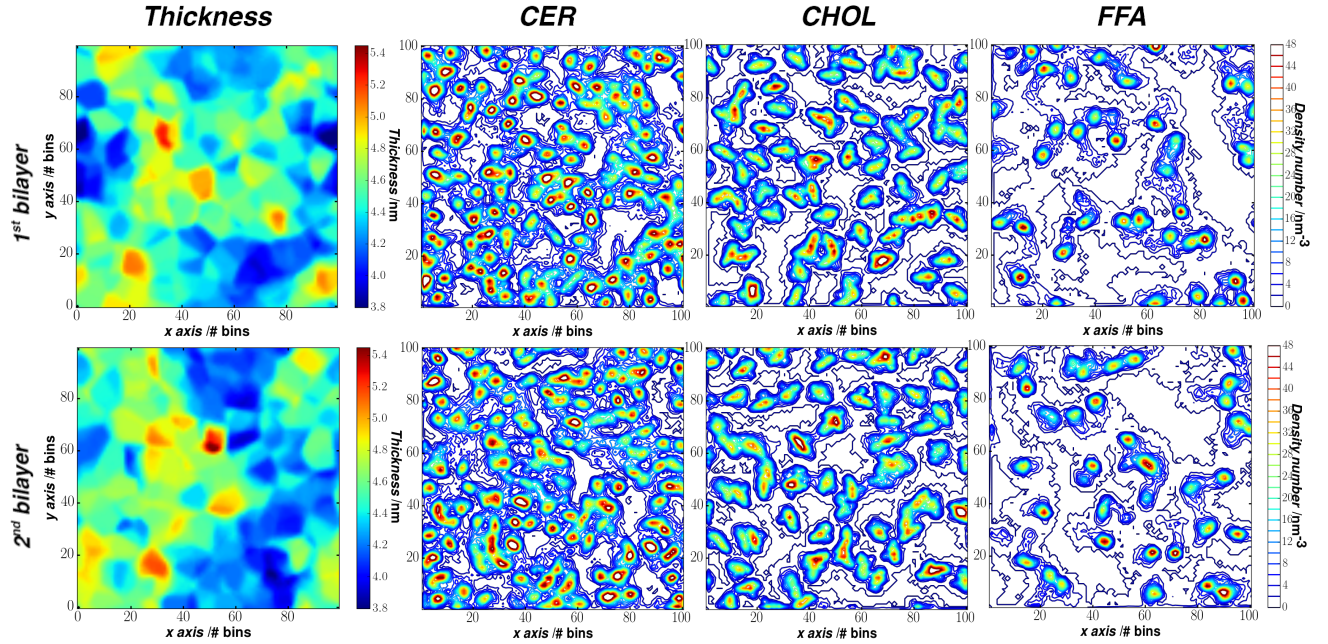


Figure S18: 2D thickness map and 2D CER[NS]24, CHOL and FFA24 number density maps are shown for sample 2, 2:2:1 LH bilayer; On the left the 2D thickness maps are shown for the bilayers composing the systems while 2D number density maps for each components are shown on the right.

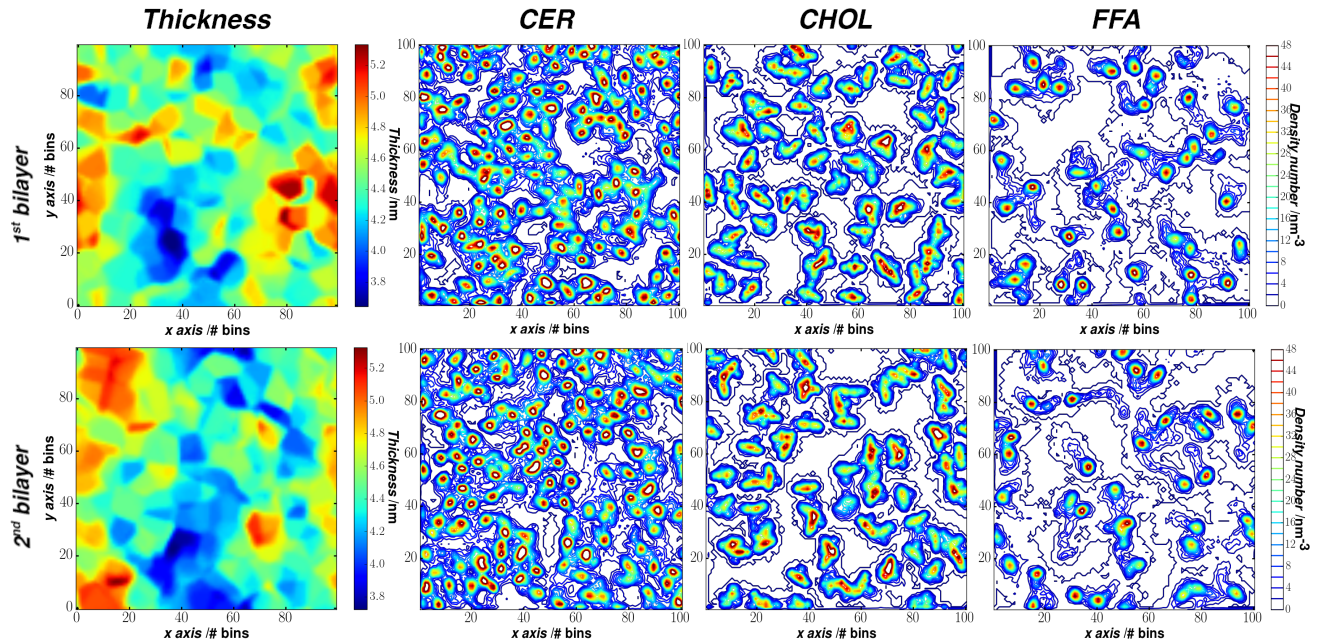


Figure S19: 2D thickness map and 2D CER[NS]24, CHOL and FFA24 number density maps are shown for sample 3, 2:2:1 LH bilayer; On the left the 2D thickness maps are shown for the bilayers composing the systems while 2D number density maps for each components are shown on the right.

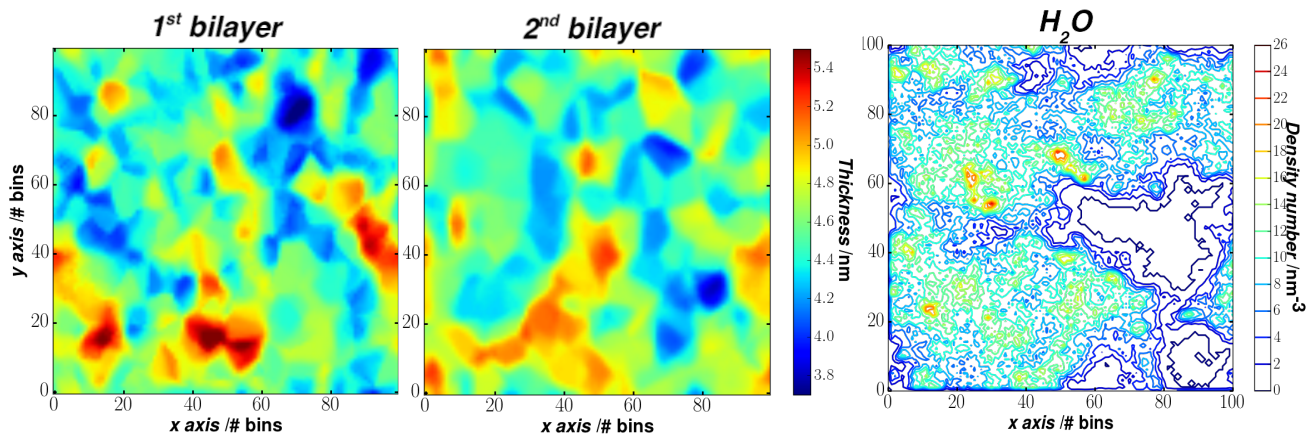


Figure S20: 2D thickness map for sample 2, 1:1:1 LH bilayer and 2D number density of the inter-layer water.

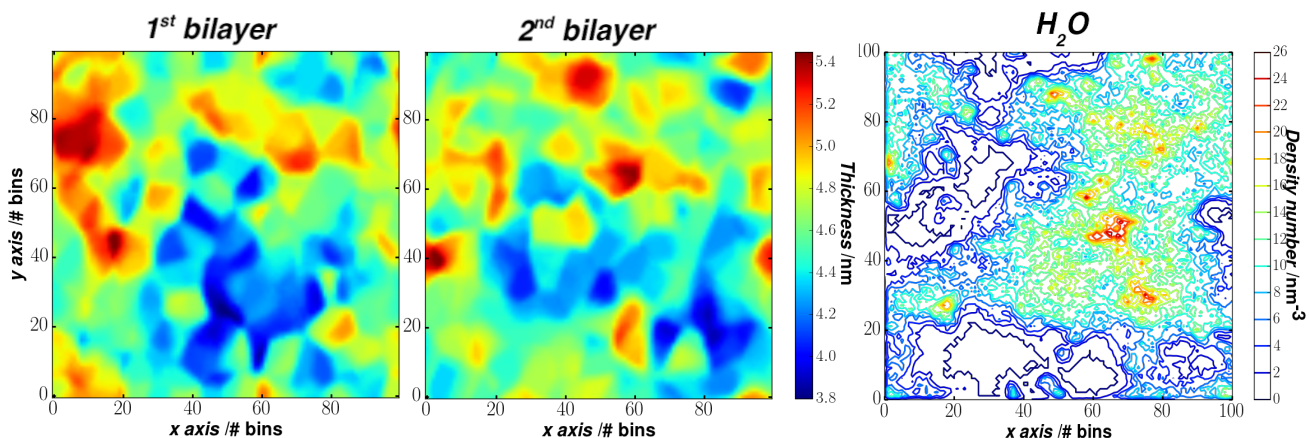


Figure S21: 2D thickness map for sample 3, 1:1:1 LH bilayer and 2D number density of the inter-layer water.

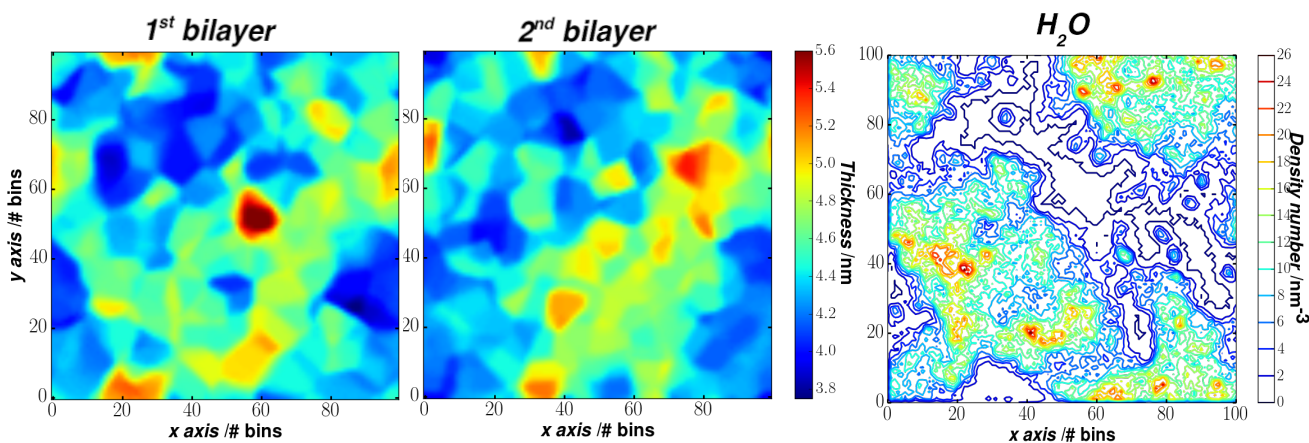


Figure S22: 2D thickness map for sample 1, 2:2:1 LH bilayer and 2D number density of the inter-layer water.

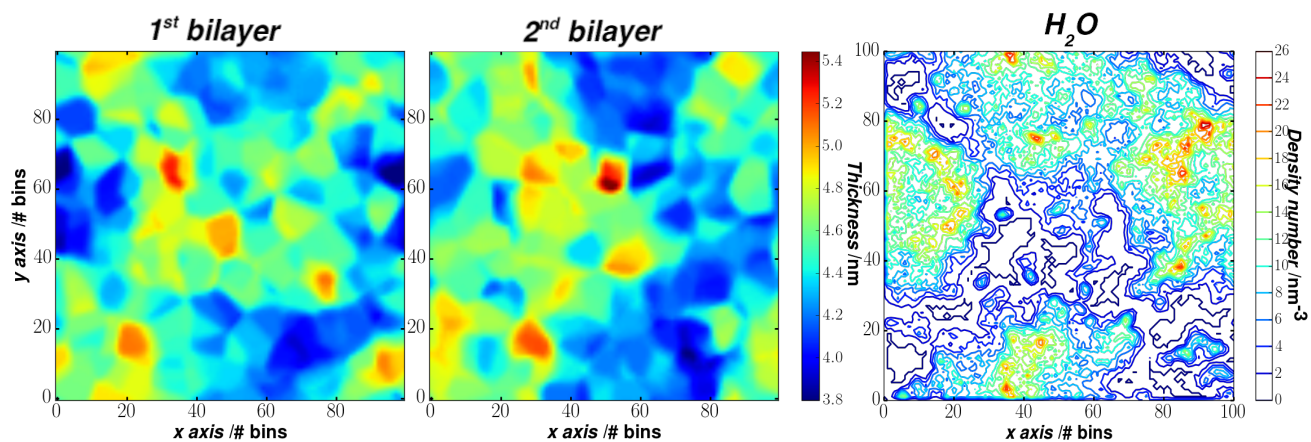


Figure S23: 2D thickness map for sample 2, 2:2:1 LH bilayer and 2D number density of the inter-layer water.

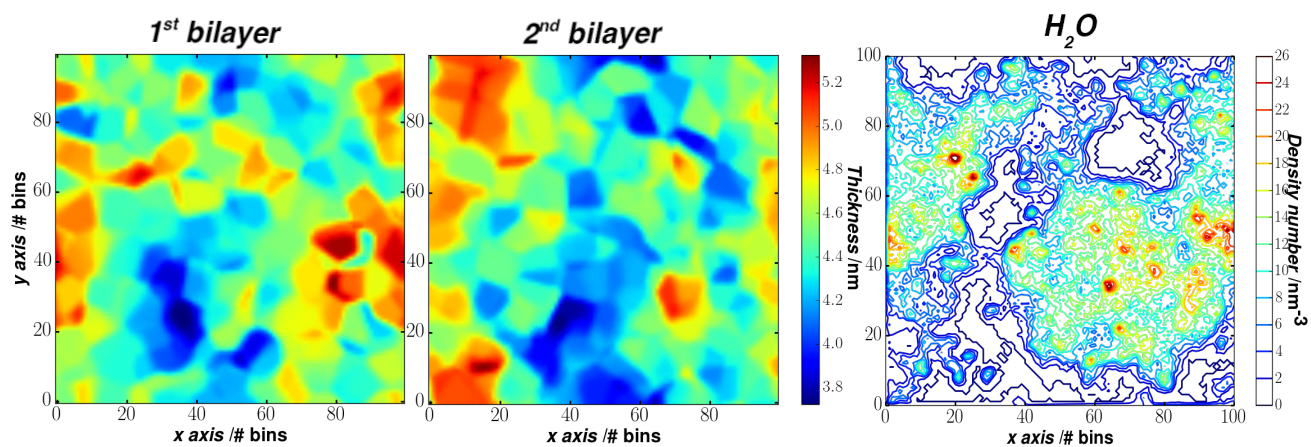


Figure S24: 2D thickness map for sample 3, 2:2:1 LH bilayer and 2D number density of the inter-layer water.

Water Pools in the 1:1:1 LH Bilayer

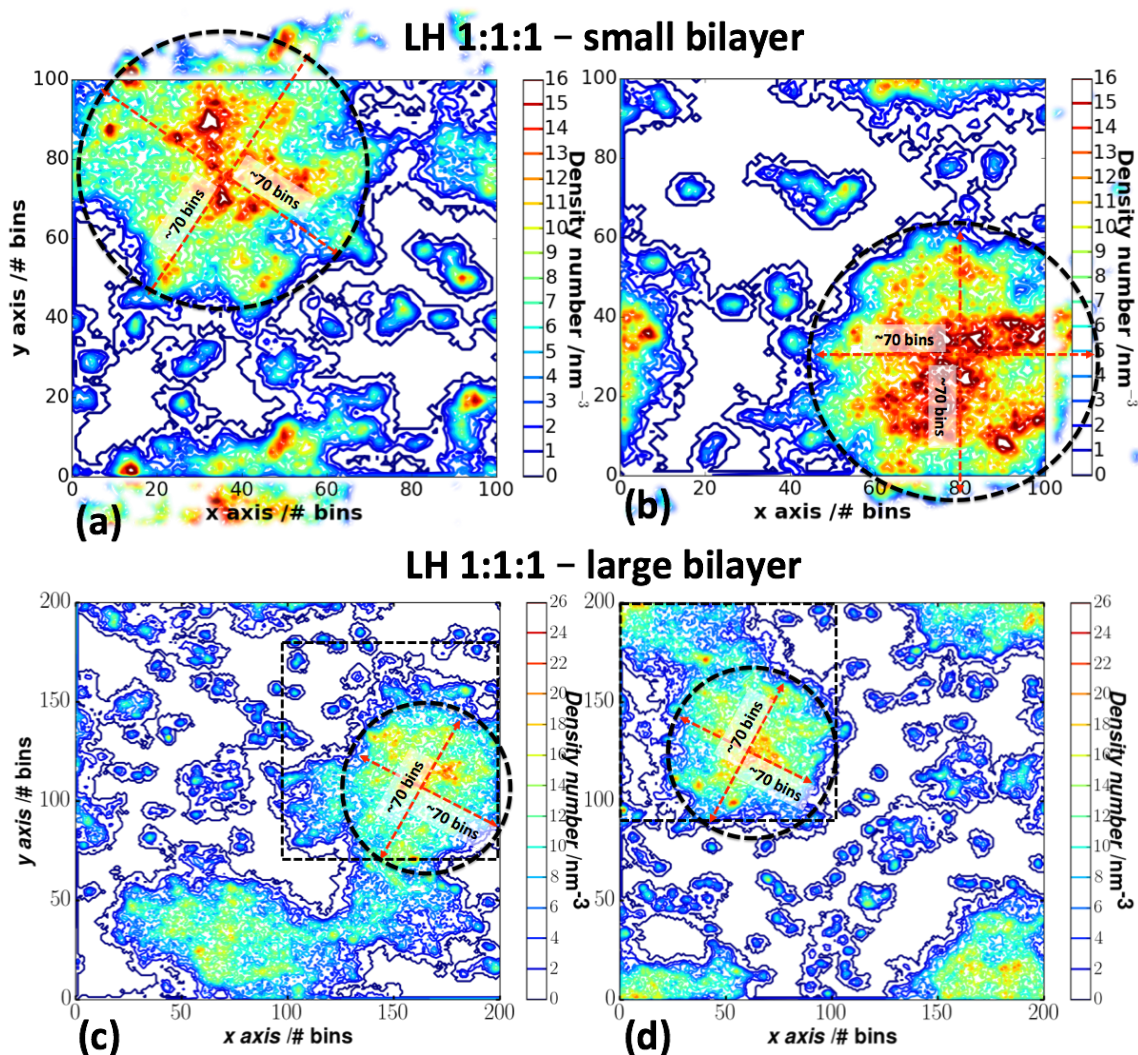


Figure S25: 2D number density maps for water in the 1:1:1 LH small ((a) and (b)) and large ((c) and (d)) bilayers. The maps show the location of the individual pools. The red arrows indicate the cross section of the water pools and an estimate of their dimensions. The black boxes in (c) and (d) indicate the size of the smaller bilayer when compared with the large one. Dotted circles were used to indicate the shape of the pools.

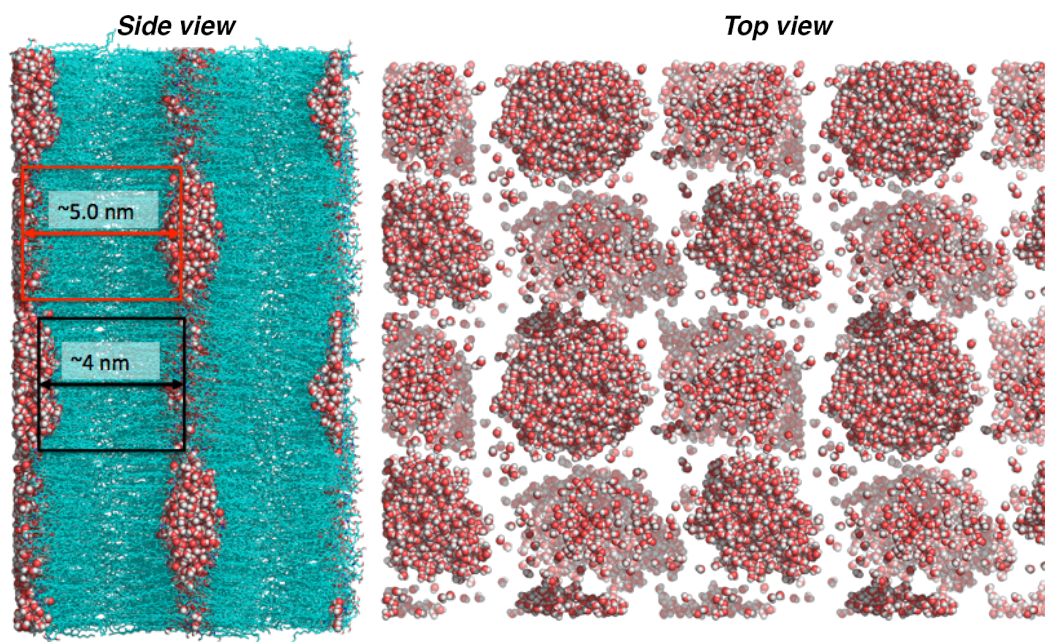


Figure S26: Snapshots of the periodic image of the larger 1:1:1 LH system after 425 ns of MD simulation at 1 bar and 305 K. On the left hand side, side view of the system; on the right hand side, top view of the system (lipids were removed for clarity). Examples of low thickness and high thickness regions are highlighted with black and red boxes respectively. Carbon atoms are coloured in cyan, oxygen in red, hydrogen in white and nitrogen in blue.

Water Permeation

1:1:1 FH bilayer

Table S4: Average composition of the 1:1:1 FH bilayer in the permeation volume around the 9 independent water molecules and correspondent Resistance (R_m) and Permeability (P). The lipid composition for each profile is reported as CER[NS]:CHOL:FFA24.

PMF plot	Ratio (%)	P ($\text{cm}^2 \text{s}^{-1}$)	R_m (s cm^{-2})
a	40.0 : 20.0 : 40.0	1.77×10^9	5.66×10^{-10}
b	11.0 : 44.5 : 44.5	3.63×10^8	2.76×10^{-9}
c	80.0 : 20.0 : 00.0	7.02×10^9	1.42×10^{-10}
d	25.0 : 25.0 : 50.0	2.50×10^9	4.00×10^{-10}
e	10.0 : 60.0 : 30.0	9.04×10^8	1.11×10^{-9}
f	25.0 : 25.0 : 50.0	1.57×10^{11}	6.37×10^{-12}
g	25.0 : 37.5 : 37.5	9.60×10^{10}	1.04×10^{-11}
h	28.6 : 42.9 : 28.6	4.71×10^9	2.12×10^{-10}
i	60.0 : 40.0 : 00.0	6.01×10^9	1.67×10^{-10}

1:1:1 LH bilayer

Table S5: Average composition of the 1:1:1 LH bilayer in the permeation volume around the 9 independent water molecules. The ratio is reported as CER[NS]24:CHOL:FFA224.

PMF plot	Ratio (%)
a	50.0 : 37.5 : 12.5
b	57.1 : 14.3 : 28.6
c	50.0 : 25.0 : 25.0
d	25.0 : 50.0 : 25.0
e	42.9 : 42.9 : 14.3
f	42.9 : 28.9 : 28.9
g	37.5 : 25.0 : 37.5
h	50.0 : 12.5 : 37.5
i	20.0 : 40.0 : 40.0

Potential of mean force (PMF) for FH models

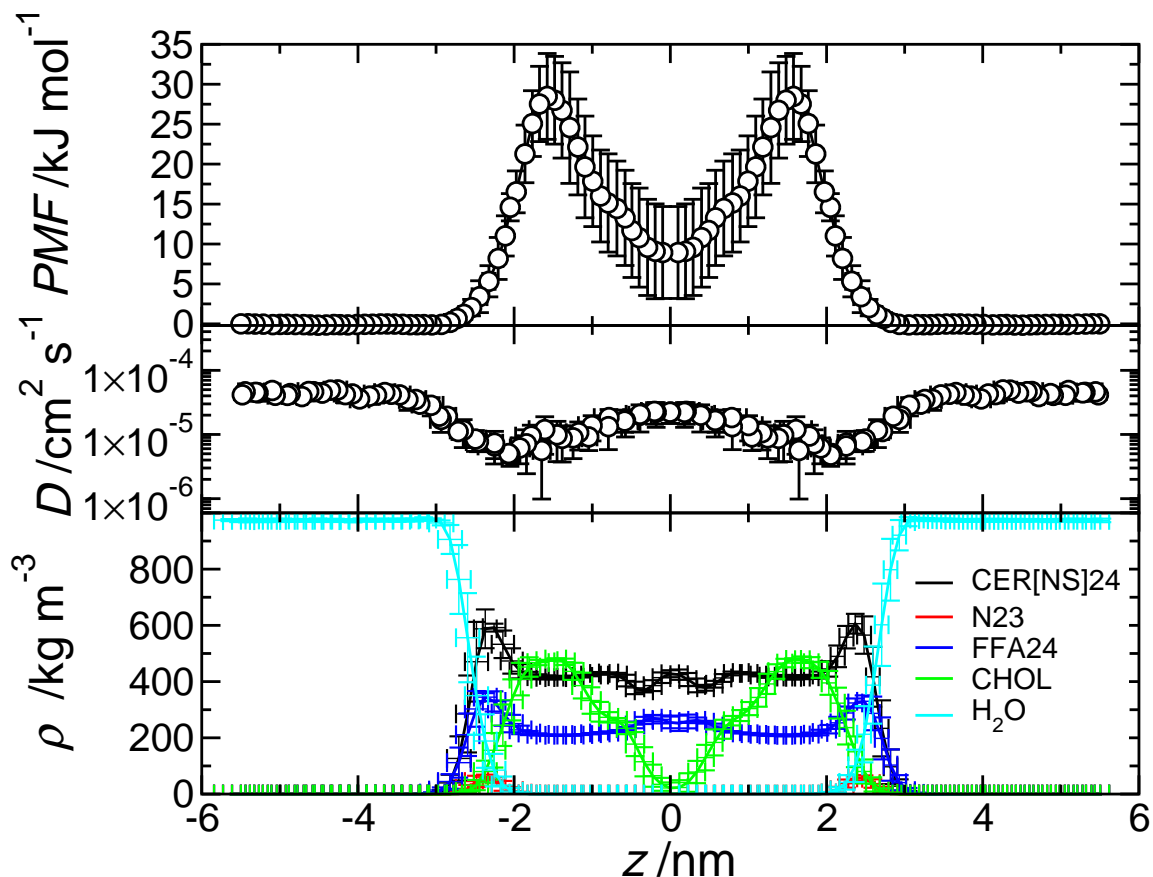


Figure S27: From the top: average PMF profile and diffusion coefficients for a water molecule at a given depth along the FH 1:1:1 bilayer at $T = 305$ K. $z = 0$ corresponds to the bilayer mid-plane. The error bars show the standard deviation obtained from nine independent samples. At the bottom, density profile for CER[NS]24, FFA24, CHOL and water. CER[NS]24 is coloured in black, N atom of the ceramide headgroup in red, CHOL in green, FFA24 in blue and water in cyan. The error bars show the standard deviation obtained from three independent simulations.

Potential of mean force (PMF) for LH models

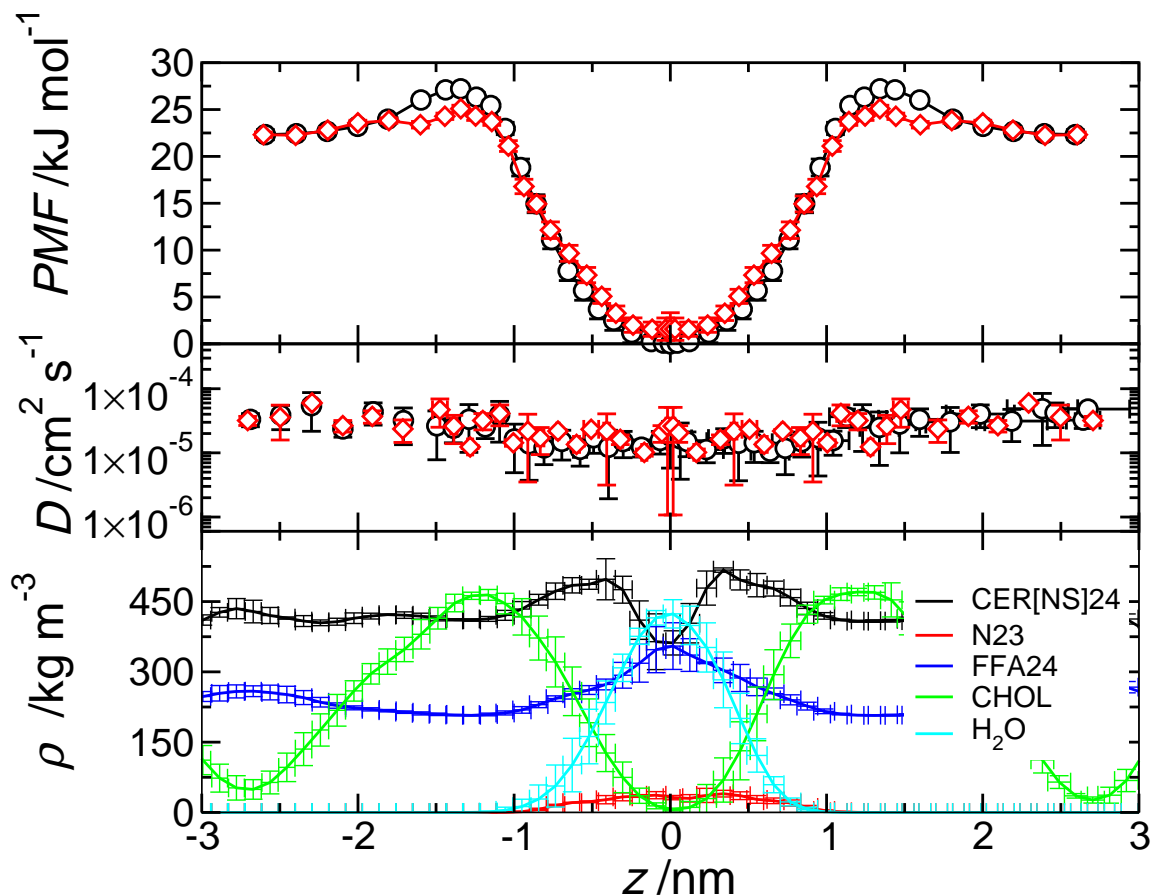


Figure S28: From the top: average PMF profile and diffusion coefficients for a water molecule at a given depth along the LH 1:1:1 bilayer at $T = 305$ K. $z = 0$ corresponds to the interface region between adjacent bilayers. The black and red lines represent the PMF profile through a wet and a dry region respectively. The error bars show the standard deviation obtained from seven (PMF profile along a wet region) and two (PMF profile along a dry region) independent samples. At the bottom, density profile for CER[NS]24, FFA24, CHOL and water. CER[NS]24 is coloured in black, N23 in red, CHOL in green, FFA24 in blue and water in cyan. The error bars show the standard deviation obtained from three independent simulations.

References

- (1) Guixà-González, R.; Rodríguez-Espigares, I.; Ramírez-Anguita, J. M.; Carrió-Gaspar, P.; Martínez-Seara, H.; Giorgino, T.; Selent, J. MEMBPLUGIN: studying membrane complexity in VMD. *Bioinformatics* **2014**, *30*, 1478–1480.
- (2) Humphrey, W.; Dalke, A.; Schulten, K. VMD – Visual Molecular Dynamics. *J. Mol. Graph.* **1996**, *14*, 33–38.
- (3) Höltje, M.; Förster, T.; Brandt, B.; Engels, T.; von Rybinski, W.; Höltje, H.-D. Molecular dynamics simulations of stratum corneum lipid models: fatty acids and cholesterol. *BBA - Biomembranes* **2001**, *1511*, 156 – 167.
- (4) Plesnar, E.; Subczynski, W. K.; Pasenkiewicz-Gierula, M. Comparative Computer Simulation Study of Cholesterol in Hydrated Unary and Binary Lipid Bilayers and in an Anhydrous Crystal. *J. Phys. Chem. B* **2013**, *117*, 8758–8769.
- (5) Das, C.; Noro, M. G.; Olmsted, P. D. Simulation Studies of Stratum Corneum Lipid Mixtures. *Biophys. J.* **2009**, *97*, 1941 – 1951.
- (6) Notman, R.; den Otter, W. K.; Noro, M. G.; Briels, W. J.; Anwar, J. The Permeability Enhancing Mechanism of DMSO in Ceramide Bilayers Simulated by Molecular Dynamics. *Biophys. J.* **2007**, *93*, 2056–2068.
- (7) Bouwstra, J.; Grams, Y.; Pilgram, G.; Koerten, H. New aspects of the skin barrier organisation assessed by diffraction and electron microscopic techniques. *Microsc. and Microanal.* **2002**, *8*, 278–279.
- (8) Das, C.; Noro, M. G.; Olmsted, P. D. Fast cholesterol flip-flop and lack of swelling in skin lipid multilayers. *Soft Matter* **2014**, *10*, 7346–7352.
- (9) van Spoel, D.; Lindahl, E.; Hess, B.; van Buuren, A. R.; Apol, E.; Meulenhoff, P. J.;

- Tieleman, D. P.; Sijbers, A. L. T. M.; Feenstra, K. A.; van Drunen, R.; Berendsen, H. J. C. Gromacs User Manual version 4.5.4, www.gromacs.org (2010).
- (10) Gapsys, V.; de Groot, B. L.; Briones, R. Computational analysis of local membrane properties. *J. Comput. Aid. Mol. Des* **2013**, *27*, 845–858.
- (11) Michaud-Agrawal, N.; Denning, E. J.; Woolf, T. B.; Beckstein, O. MDAAnalysis: A toolkit for the analysis of molecular dynamics simulations. *J. Comput. Chem.* **2011**, *32*, 2319–2327.
- (12) Hagberg, A. A.; Schult, D. A.; Swart, P. J. Exploring Network Structure, Dynamics, and Function using NetworkX. Proceedings of the 7th Python in Science Conference. Pasadena, CA USA, 2008; pp 11 – 15.
- (13) Hunter, J. D. Matplotlib: A 2D graphics environment. *Comput. Sci. Eng.* **2007**, *9*, 90–95.